Nanoporous hydrogenated TiO$_2$ photocatalysts generated by underwater discharge plasma treatment for solar photocatalytic applications

Ha-Rim An [a,1], So Young Park [a,1], Jin Young Huh [b,c], Hyeran Kim [a], Young-Chul Lee [d], Young Boo Lee [e], Yong Cheol Hong [b,f,**], Hyun Uk Lee [a,*]

[a] *Advanced Nano-surface Research Group, Korea Basic Science Institute, Daejeon 305-806, Republic of Korea*
[b] *Plasma Technology Research Center, National Fusion Research Institue, Gunsan 573-540, Republic of Korea*
[c] *Department of Electrical and Biological Physics, Kwangwoon University, Seoul 131-701, Republic of Korea*
[d] *Department of BioNano Technology, Gachon University, Gyeonggi-do 13120, Republic of Korea*
[e] *Jeonju Center, Korea Basic Science Institute, Jeonju 561-756, Republic of Korea*
[f] *NPAC, Daejeon 305-806, Republic of Korea*

ARTICLE INFO

ABSTRACT

In this paper, we report on the mass production, characteristics and application of a hydrogenated TiO$_2$ photocatalyst (H-TiO$_2$) with high reactivity under solar light irradiation. The H-TiO$_2$ photocatalyst has been prepared by simple sol-gel method/underwater discharge plasma treatment at room temperature and atmospheric pressure. The optical absorption spectrum of TiO$_2$ can be extended from the ultraviolet (UV) into the visible range by changing the surface properties. The crystallinity, hydrogenation and porosity of TiO$_2$ can be greatly enhanced within 90 s through underwater discharge plasma, using amorphous TiO$_2$ (as-synthesized TiO$_2$, a-TiO$_2$) as the precursor. The resultant H-TiO$_2$ showed high bicrystalline (anatase/brookite phases) and a large surface area (267.5 m^2/g), thus improving photocatalytic activity. We have demonstrated that H-TiO$_2$ showed significant photocatalytic efficiencies for degradation of reactive black 5, rhodamine B, and phenol under solar light irradiation, up to 10 times higher than those of commercial TiO$_2$ and a-TiO$_2$, leading to complete water purification. Interestingly, the H-TiO$_2$ photocatalyst also exhibited strong antimicrobial activities against Gram-negative *Escherichia coli* and Gram-positive *Staphylococcus aureus* under solar light irradiation, up to 5-times greater than those of commercial TiO$_2$ and a-TiO$_2$. Given that H-TiO$_2$ can be mass produced and easily processed by underwater discharge plasma, we expect this plasma technology may find important environmental and medical applications.

1. Introduction

Titanium dioxide (TiO$_2$) has received much interest for environmental applications including photocatalytic hydrogen generation and pollutant removal, due to its strong optical absorption, chemical stability, low cost and high reactivity [1–5]. TiO$_2$ has large electronic bandgaps of 3.0–3.2 eV, which restrict its optical absorption mainly to the ultraviolet (UV) region, corresponding to less than 4% of natural solar energy. Therefore, the overall solar activation of TiO$_2$ is limited even if TiO$_2$ is very effective in utilizing UV light. For this reason, much effort has been devoted to improving the visible light absorption of TiO$_2$ over many years [6–9]. For example, studies have been conducted on the incorporation of light absorbing materials (sensitizer, quantum dots, and dyes) and the modification of TiO$_2$ electronic properties by the addition of external dopants (transition metals, nitrogen, sulfur, and phosphorus) [10–15]. Among these strategies, tuning TiO$_2$ with hydrogenation also has attracted considerable attention [16–18]. Chen et al. reported that hydrogenated TiO$_2$ expands the excitation wavelength range toward the visible light region, reduces recombi-

nation centers, and increases the lifetime of holes [19]. The methods for fabricating hydrogenated TiO_2 mostly rely on the reduction of Ti^{4+} to Ti^{3+} by thermal treatment under hydrogen or reducing conditions, and high-energy electron, argon, or hydrogen plasmas that inevitably require high temperatures, a costly vacuum system, complicated multiple steps, and a long processing time [19–23]. Thus, it is desirable to develop a facile method for the fabrication of hydrogenated TiO_2.

In this study, we prepared hydrogenated nanoporous TiO_2 (H-TiO_2) photocatalysts using an underwater discharge plasma system, which is a simple, fast, and mass-producible method operated at room temperature and atmospheric pressure, using underwater electrical discharges generated in a narrow capillary tube. This approach has recently received substantial attention as it can serve as a water purification tool for environmental cleanup activities and may be applicable to the elimination of airborne microorganisms [24–26]. Furthermore, a considerable number of studies have reported results involving discharges on or in water, including water treatment or decontamination [27,28], bacteria disinfection [29,30], surgical application [31], and material synthesis application [32]. These applications are enabled by numerous active plasma chemistry reactions that are not normally observed in an aqueous solution, promoted by, e.g., reactive radicals, charged particles, ultraviolet light, and shockwaves [24].

Discharge in and on water can initiate a variety of plasma-chemical effects, and a number of primary and secondary species can be formed by these discharges in the gas phase and at the gas-water interface [31]. In view of this, we specially designed the underwater plasma electrode system to sustain a stable discharge with an oxygen gas flow in water. We hypothesized that the plasma electrode system could synthesize the highly crystalline H-TiO_2 from amorphous TiO_2 (a-TiO_2), incorporating atomic hydrogen and hydroxyl molecules produced from water dissociation into its surface. Simultaneously, reactive oxygen species could oxidize carbon species present on the TiO_2 surface, thereby increasing its specific surface area. As a result, the high crystallinity (anatase/rutile bicrystalline) and large responsive surface area obtained via the underwater plasma process contribute to a ten-fold increase in the H-TiO_2 photocatalytic efficiency for degradation of organic compounds in water, and a five-fold increase in efficiency for sterilization of Gram-negative *Escherichia coli* and Gram-positive *Staphylococcus aureus* compared to other commercial TiO_2 (P25) and a-TiO_2 photocatalysts.

2. Experimental

2.1. Fabrication of H-TiO_2 photocatalysts

Nanoporous hydrogenated TiO_2 (H-TiO_2) photocatalysts were fabricated via a combination of a simple sol-gel process and underwater discharge plasma treatment. All the reagents for the synthesis of H-TiO_2 photocatalysts were prepared without further purification. First, a solution containing 5 mol titanium(IV) butoxide (170 g, $Ti(OC(CH_3)_3)_4$, Sigma-Aldrich, USA) and 0.5 mol hexadecyltrimethylammonium bromide (18.2 g, CTAB, $C_{16}H_{33}N(CH_3)_3Br$, Sigma-Aldrich, USA) in 100 ml deionized water was used to prepare TiO_2 nanoparticles. The particles in the solution were then well dispersed by stirring for 30 min and allowing to stand for 4 h. The precipitate obtained from the cloudy solution was separated and washed several times with deionized water and dried at room temperature. The amorphous TiO_2 (a-TiO_2) were synthesized according to our previous literature report [33]. From this process, 123.1 g of a-TiO_2 could be obtained and the yield was estimated to be 71.4%. The yield of the sol-gel reaction was calculated
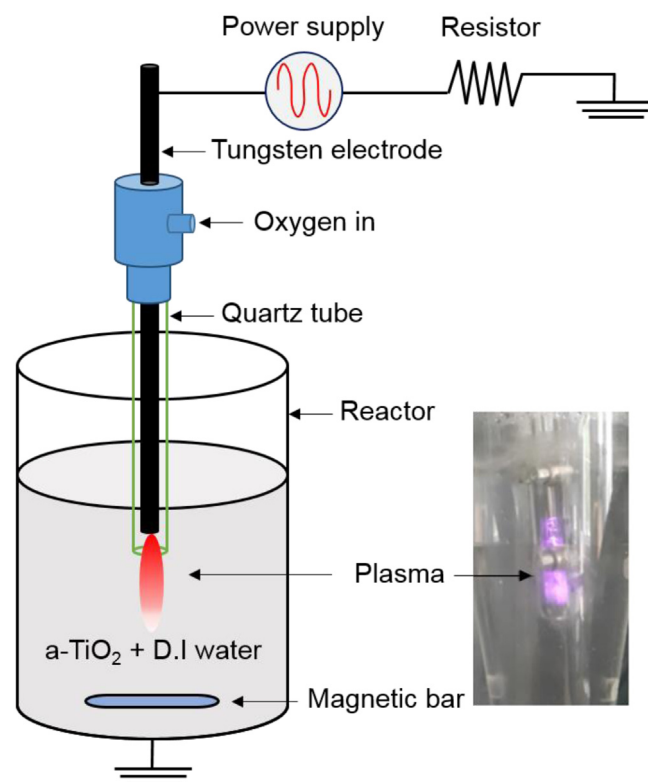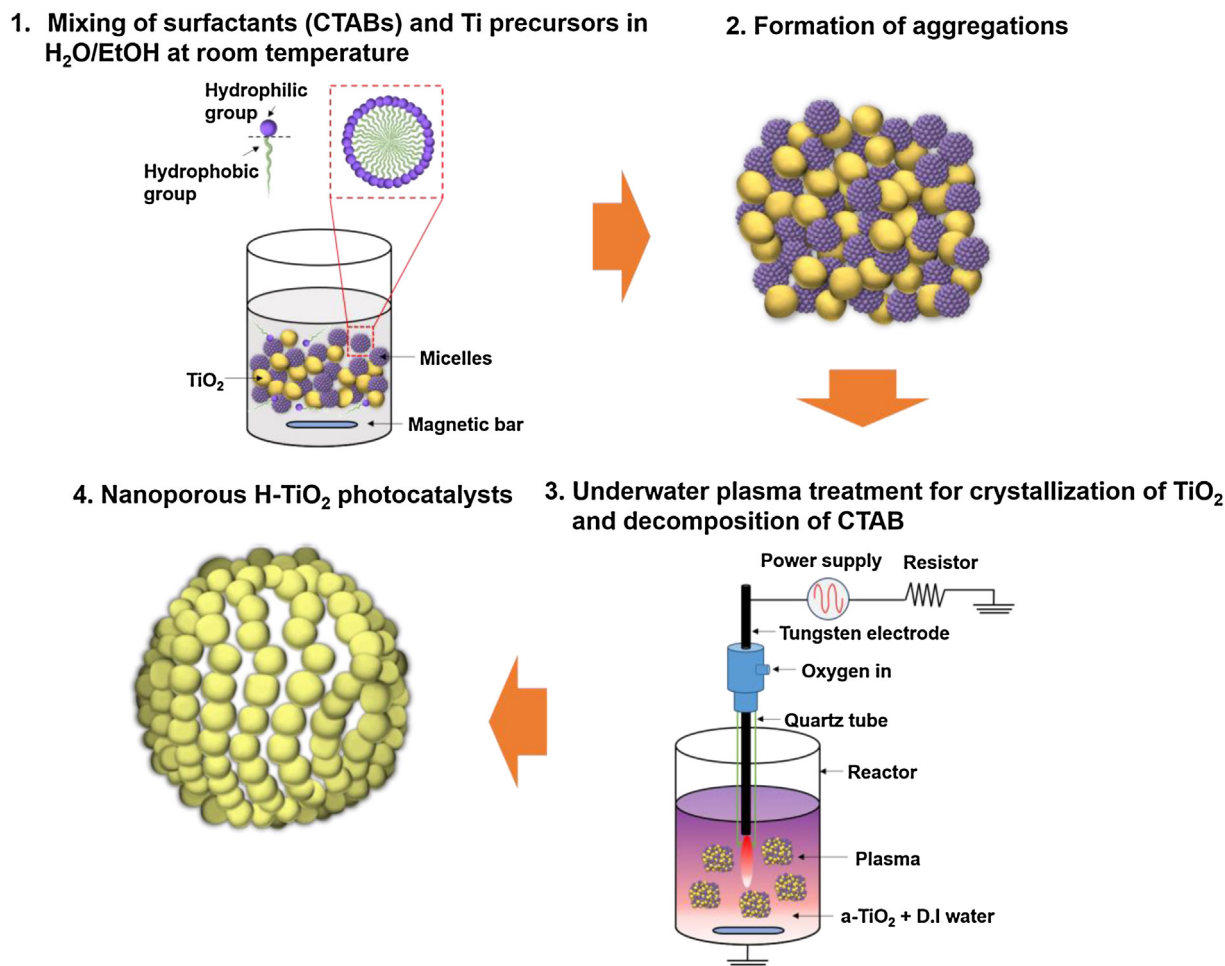

Scheme. 1. Schematic presentation of experimental set-up for synthesis of hydrogenated nanoporous TiO_2 (H-TiO_2) photocatalysts.

on the basis of initial raw materials weight taken and weight of end product fabricated after the treatment.

Scheme 1 shows the schematic presentation of experimental set-up for the synthesis of H-TiO_2. The dried a-TiO_2 nanoparticles (15 g, as-synthesized TiO_2) were dispersed with deionized water (400 ml). The suspension was then treated with the underwater discharge plasma in a vessel. As shown in Scheme 1, the plasma treatment system (manufactured by NPAC Co., Korea) consists of a power supply operated at 20 kHz, a plasma electrode system with a gas injection channel, and a reactor. In the plasma electrode system, the tungsten electrode with a diameter of 9.5 mm was tightly inserted into a quartz tube with an inner diameter of 10 mm. The distance between the ends of the tungsten electrode and the quartz tube was approximately 10 mm. Oxygen gas at the flow rate of one liter per minute was introduced into the narrow gap formed between the metal electrode and the dielectric tube. The inset of Scheme 1 shows the discharge plasma image during operation. The applied plasma power was approximately 90 W at the discharge voltage of 13 kV. During plasma treatment, the vessel was constantly stirred by a magnetic bar. The underwater plasma treatment time was controlled within the 0–7 min range. We labelled the resulting nanoporous hydrogenated TiO_2 (H-TiO_2) treated for 1.5 min, 3 min, 5 min, and 7 min, as H-TiO_2-1.5, H-TiO_2-3, H-TiO_2-5, and H-TiO_2-7, respectively.

2.2. Characterization of H-TiO_2 hybrid photocatalysts

The morphology and size distribution of the H-TiO_2 samples were characterized by FE-SEM (Hitachi; S-4700, Japan) and HR-TEM (JEOL JEM 2200, Japan). For the analyses, samples were placed on the surface of a copper grid and dried under ambient conditions. Surface properties including the respective Brunauer-Emmett-Teller (BET) surface areas, pore volumes, and pore diameters of the H-TiO_2 samples were estimated using a BET analyzer (Micromerit-

1. Mixing of surfactants (CTABs) and Ti precursors in H$_2$O/EtOH at room temperature

2. Formation of aggregations

4. Nanoporous H-TiO$_2$ photocatalysts

3. Underwater plasma treatment for crystallization of TiO$_2$ and decomposition of CTAB

Scheme. 2. Schematic diagrams of formation mechanism of H-TiO$_2$ photocatalysts.

ics ASAP 2020, USA). To investigate the crystalline structures of the H-TiO$_2$ samples, XRD (Rigaku RDA-cA X-ray diffractometer equipped with Cu Kα radiation, Japan) was used. Raman spectroscopy (Renishaw RM1000-Invia, UK) was performed in a backscattering configuration excited with a visible laser (wavelength = 514 nm), a notch filter cut-off frequency of 50 cm^{-1}, and a focus-spot size of 5 μm. Spectra were obtained through a × 100 objective lens and recorded on 1800 lines per mm^{-1} grating providing a spectral resolution of ≈1 cm^{-1}. To avoid laser-induced heating and ablation of the samples, all of the spectra were recorded at low power levels (≈0.1 mW) and over short integration times (≈5 s). X-ray photoelectron spectroscopy (XPS) and UV photoelectron spectroscopy (UPS) measurements were carried out using AXIS Ultra DLD (Kratos, UK) equipped with monochromatic Al Kα (1486.6 eV) as an X-ray source and He I gas (21.22 eV) as a UV source. All the XPS peak positions resulting from relative surface charging were adjusted using the C 1s level at 284.6 eV as an internal standard. Thermogravimetric analysis-differential scanning calorimetry (TGA-DSC) studies were also conducted using Q600 SDT (TA instruments, USA) from room temperature to 800 °C with a heating rate 10 °C/min in N$_2$ (100 ml/min) atmosphere. In order to detect free-radicals using the spin trap agent 5,5-dimethyl-1-pyrroline N-oxide (DMPO; 0.3 M in PBS buffer at pH 7.2, Sigma-Aldrich, USA), an aliquot of as-prepared sample (100 μL of 5 mg TiO$_2$ sample mixed with 300 μL DMPO solution) was filled into a capillary tube and directly irradiated with a light emitting diode (LED) (>400 nm) source for 5 min. The results were recorded by an ESR spectrometer (JEOL JES-FA200, Japan; center field: 327 mT;

power: 1 mW; amplitude: 5.0 × 100; modulation width: 0.4 × 1; sweep width: 1 × 10; sweep time: 30 s).

2.3. Measurement of photocatalytic and antibacterial activities

The photocatalytic degradation tests of reactive black 5 (RB 5; 3 mg/L, Sigma-Aldrich, USA), rhodamine B (Rho B; 3 mg/L, Sigma-Aldrich, USA), and phenol (Ph; 1.88 mg/L, Aldrich, USA) solutions containing H-TiO$_2$ samples (0.5 g/L) were performed under UV (4 W, 365 nm, VSLAB VL-4CL, Korea) and solar light (150 W Xe lamp, 200 nm > λ, SCHOTT, USA) irradiation, and absorbances of the resulting solutions were measured by using a UV-VIS-IR spectrophotometer (Varian, Cary5000, Australia) in the 200–800 nm region. The concentrations of the degraded RB 5, Rho B, and Ph solutions were estimated from the peak intensities of the absorbances at 598 and 664 nm, respectively. The change in the RB 5, Rho B, and Ph concentration ($\ln(C_0/C) = kt$, where k is the apparent reaction rate constant, and C_0 and C are the initial and reaction concentrations of the different reagents) with various reaction times (0–120 min) was also investigated. Also, H-TiO$_2$ samples were recycled to determine the stability of the photocatalysts. This recycling test of the photocatalytic activity of the H-TiO$_2$ samples was conducted after washing the samples with deionized water and drying in an oven (60 °C) for 6 h after each cycle.

The antibacterial activities of different concentrations of H-TiO$_2$ samples were evaluated by determining the inhibition of Gram-negative *E. coli* and Gram-positive *S. aureus* bacteria, under fluorescent irradiation at room temperature, by measurement of
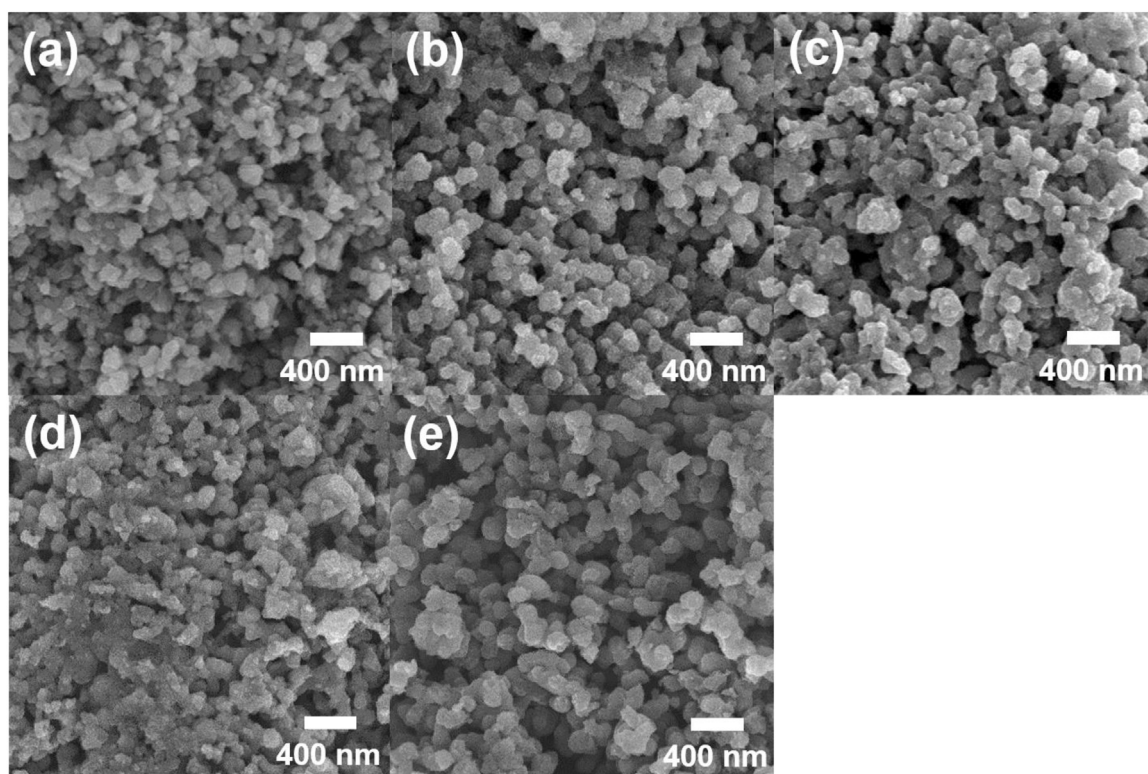
Fig. 1. FESEM images of (a) as-synthesized TiO_2 (a-TiO_2), (b) H-TiO_2-1.5 (underwater discharge plasma treatment time: 90 s), (c) H-TiO_2-3 (3 min), (d) H-TiO_2-5 (5 min) and (e) H-TiO_2-7 (7 min).

the percent viability (% survival). The nanoparticle suspensions were prepared with different concentrations, i.e., 10, 25, 50, 75 and 100 mg in 25 ml of a bacterial culture having 0.2 optical density (O.D.) at 660 nm and stirred for 6 h under fluorescent light (2 fluorescent lights × 40 W). The mixture of nanoparticles and bacterial culture was spread over Luria agar plates, and the viability of the bacterial cells was determined by its colony forming ability.

For the photocatalytic activity and antimicrobial tests, the data were averaged and expressed as the mean ± standard deviation. Each test was repeated up to four times. Statistical analysis was performed using analysis of variance (ANOVA), with p-values < 0.05 considered as significant.

3. Results and discussion

3.1. Physicochemical, structural, and optical characterization, and proposed H-TiO_2 formation mechanism

Scheme 2 illustrates our approach in this study to develop a facile strategy for efficient mass production of hydrogenated TiO_2 (H-TiO_2) nanoparticles with a large surface area. We prepared nanoporous H-TiO_2 through the interaction between CTAB as a surfactant and titanium(IV) butoxide as a TiO_2 precursor, without any additional heat treatment process. The subsequent processing for H-TiO_2 preparation involves the following steps: (i) CTAB, used to produce micelles as templates for the formation of nanoporous structures, is dissolved in de-ionized water; (ii) the TiO_2 precursor is added to the surfactant solution in a simple sol-gel process; (iii) this mixture is treated with the underwater plasma to remove the micelles and crystallize the structure of TiO_2; (iv) the extreme energy input of the underwater plasma leads to highly crystallized and hydrogenated TiO_2 with large surface area.

Fig. 1 show the field emission scanning electron microscopy (FESEM) images obtained from a-TiO_2 and H-TiO_2 samples. All the TiO_2 samples are observed as rounded or randomly shaped aggregates consisting of small particles. The aggregate sizes were almost unchanged after the underwater plasma treatment and all TiO_2 samples displayed similar aggregate sizes of 110–170 nm. This aggregation phenomenon can be attributed to the fast condensation of TiO_2 nanoparticles by the high-energy underwater plasma, that results in rounded or randomly shaped aggregated particles (See Fig. S1 for high magnification SEM images).

To conduct further morphological observation and investigate the crystalline nature of the TiO_2 samples, high-resolution TEM (HRTEM) analysis was employed. As shown in Fig. 2a–e, HRTEM images confirm that H-TiO_2 samples are composed of aggregated nanocrystalline anatase/brookite with high crystallinity, and crystallite sizes of ∼5–7 nm. Superior crystallization of H-TiO_2 was induced by the high energy conditions of the underwater plasma [15]. Also, the observation of cloudy and unclear areas between crystallized TiO_2 grains implies that a few micelles remaining inside TiO_2 aggregates are present in amorphous states. In addition, the observed lattice spacing was determined as 0.35 nm in all samples, corresponding to (101) plane of the anatase poly-crystal phase [15,34–36].

In order to examine the pore distributions of the TiO_2 samples, a BET analyzer was used. In Table 1, the BET surface areas were 37.0 m^2/g for commercial TiO_2 (P25), 53.5 m^2/g for a-TiO_2, 267.5 m^2/g for H-TiO_2-1.5, 262.6 m^2/g for H-TiO_2-3, 261.2 m^2/g for H-TiO_2-5, and 262.2 m^2/g for H-TiO_2-7. The BET values of the H-TiO_2 samples were significantly higher than those of the commercial TiO_2 and a-TiO_2, and remained constant due to similar sizes, total pore volume and mean pore diameter of H-TiO_2 samples. It can be seen that among different durations for underwater plasma treatment, the shortest duration results in the formation of a slightly larger number of nanopores. This result is consistent
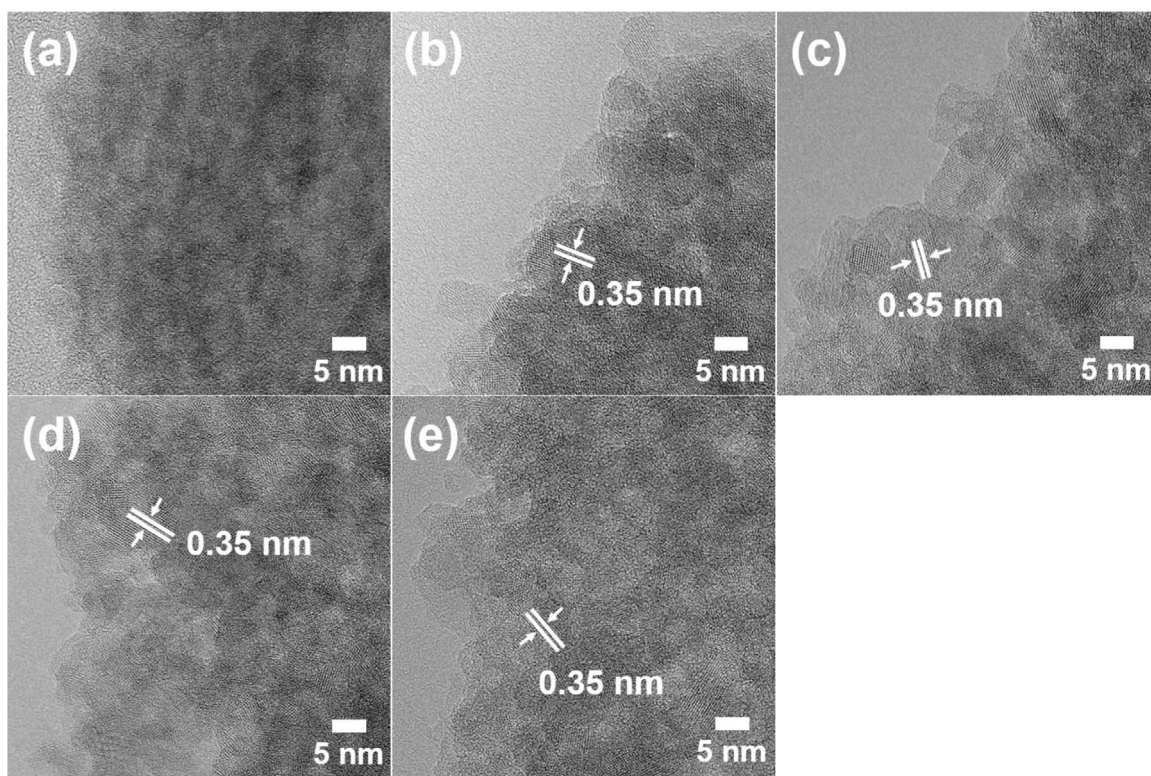
Fig. 2. HR-TEM images of (a) a-TiO$_2$, (b) H-TiO$_2$-1.5, (c) H-TiO$_2$-3, (d) H-TiO$_2$-5 and (e) H-TiO$_2$-7.

Table 1
Underwater plasma effects on BET, pore volume and size of commercial TiO$_2$ (P25), a-TiO$_2$, H-TiO$_2$-1.5, H-TiO$_2$-3, H-TiO$_2$-5, and H-TiO$_2$-7.

	P25	a-TiO$_2$	H-TiO$_2$-1.5	H-TiO$_2$-3	H-TiO$_2$-5	H-TiO$_2$-7
BET (m^2/g)	37.0	53.5	267.5	262.6	261.2	262.2
Total pore volume (cm^3/g)	0.018	0.076	0.138	0.135	0.134	0.135
Mean pore diameter (nm)	1.99	1.99	2.06	2.06	2.05	2.05

with our expectation illustrated in Scheme 2 that CTAB micelles are decomposed during underwater plasma treatment and many nanopores are formed in the TiO$_2$, resulting in a nanoporous structure. That is, the underwater plasma had effects on the BET surface area and pore size distribution, which correlate with photocatalytic and antibacterial activities.

To reconfirm the crystal structures of a-TiO$_2$, H-TiO$_2$-1.5, H-TiO$_2$-3, H-TiO$_2$-5, and H-TiO$_2$-7, X-ray diffraction (XRD) pattern and Raman spectrum were analyzed. As shown in Fig. 3a, the XRD spectrum of a-TiO$_2$ sample presents somewhat weak and broad peaks and the characteristic peaks of final samples were observed at 2θ = 25.3°, 37.8°, 47.8°, 54.4°, and 62.9°, corresponding to the (101), (004), (200), (105), and (204) planes of anatase TiO$_2$ phases (space group I4$_1$/amd, JCPDS card No. 84-1286), respectively, and at 30.5° corresponding to the (002) plane of the brookite TiO$_2$ phases (space group P*cab*, JCPDS card No. 12-1360) [15,33]. From the corresponding XRD main peak areas of samples, the percentage of anatase and brookite could be calculated [37,38]. The H-TiO$_2$ samples consist of ~92.2–93.3% of anatase and ~6.7–7.8% of brookite. The ratios were not significantly affected by the underwater plasma treatment time. The peak intensities of H-TiO$_2$ samples were increased compared with the a-TiO$_2$ and were similarly maintained in all the H-TiO$_2$ samples. This shows that highly crystalline TiO$_2$ could be obtained under all durations of underwater plasma treatment time, 90 s to 7 min. Therefore, the XRD results indicated that all the H-TiO$_2$ samples were composed of anatase/brookite phases and that high energy reactions of underwater plasma species on TiO$_2$

Table 2
Chemical compositions of a-TiO$_2$, H-TiO$_2$-1.5, H-TiO$_2$-3, H-TiO$_2$-5, and H-TiO$_2$-7.

Atomic%	a-TiO$_2$	H-TiO$_2$-1.5	H-TiO$_2$-3	H-TiO$_2$-5	H-TiO$_2$-7
C	56.0	42.4	37.8	36.2	32.4
O	34.3	41.9	45.2	45.2	48.6
Ti	9.7	15.7	17.0	18.6	19.0

improved the crystallinity of a-TiO$_2$ [33,36]. Raman spectroscopy supported the same conclusion (Fig. 3b). According to factor group analysis, anatase has six Raman active modes (A$_{1g}$ + 2B$_{1g}$ + 3E$_g$), which appear at 144 cm^{-1} (E$_g$), 197 cm^{-1} (E$_g$), 399 cm^{-1} (B$_{1g}$), 513 cm^{-1} (A$_{1g}$), 519 cm^{-1} (B$_{1g}$), and 639 cm^{-1} (E$_g$) [39,40]. From the positions and intensities of the Raman peaks, therefore, it is shown that H-TiO$_2$ samples are composed of anatase TiO$_2$ and exhibit high crystallinity. Consequently, the Raman spectra results were consistent with the XRD results, which indicate that the H-TiO$_2$ samples are composed of a highly crystalline anatase/brookite phase.

To investigate the effect of underwater plasma on the chemical bonding states of TiO$_2$, X-ray photoelectron spectroscopy (XPS) was carried out. As shown in Fig. 4, C 1s, O 1s, and Ti 2p were observed from all the TiO$_2$ samples, including a-TiO$_2$, H-TiO$_2$-1.5, H-TiO$_2$-3, H-TiO$_2$-5, and H-TiO$_2$-7. In addition, the chemical compositions listed in Table 2 show that the atomic concentrations of C 1s of H-TiO$_2$ samples were lower than that of a-TiO$_2$. This indicates that the underwater plasma causes the degradation of CTAB, liberating a large amount of carbon. The same results could be seen from Thermogravimetric analysis (TGA) curves. The TGA
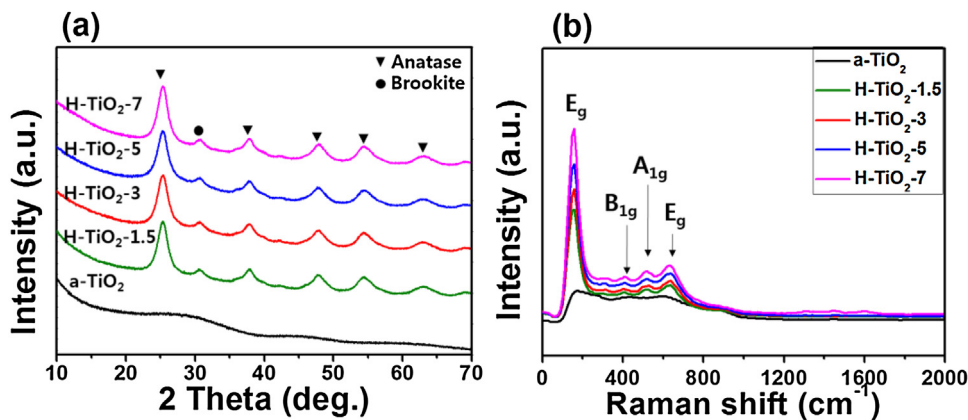
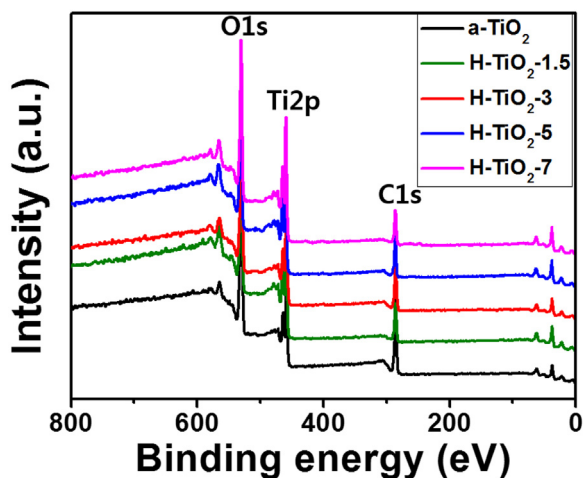**Fig. 3.** (a) XRD patterns and (b) Raman spectra of a-TiO$_2$, H-TiO$_2$-1.5, H-TiO$_2$-3, H-TiO$_2$-5 and H-TiO$_2$-7.

Fig. 4. Wide-scan XPS spectra of a-TiO$_2$, H-TiO$_2$-1.5, H-TiO$_2$-3, H-TiO$_2$-5 and H-TiO$_2$-7.

curves were measured to examine the residual of surfactant. As shown in Fig. S2, the TGA curve of a-TiO$_2$ showed more than 46% weight loss from 30–100 °C corresponding to the removal of water or some organic molecules and showed 4% weight loss from 200–600 °C, which was owing to the decomposition of oxygen and carbon group. Compared with a-TiO$_2$, H-TiO$_2$ samples exhibited 7–13% weight loss from 30–100 °C and 8–10% weight loss appearing at 200–600 °C. This indicates that the surfactant was sufficiently eliminated during underwater plasma treatment [41], which is consistent with XPS results. The high-resolution XPS spectra of the Ti 2p core level obtained from a-TiO$_2$, H-TiO$_2$-1.5, H-TiO$_2$-3, H-TiO$_2$-5, and H-TiO$_2$-7 are plotted in Fig. 5a–e. The Ti 2p$_{3/2}$ peaks of all the TiO$_2$ samples are separated into two or three broad peaks, which center at ∼458.6 eV, ∼457.8 eV, and ∼459.8 eV corresponding to TiO$_2$, Ti$_2$O$_3$, and Ti(OH)$_4$, respectively [4,5,42]. The ratios of TiO$_2$/(TiO$_2$ + Ti$_2$O$_3$ + Ti(OH)$_4$) calculated from the corresponding Ti 2p peak areas were ∼95.1% for a-TiO$_2$ and ∼87.1 to 78.0% for H-TiO$_2$ samples (Table S1), suggesting that more oxygen vacancies (Ti^{3+} sites) and hydroxyl species exist on the surface of H-TiO$_2$
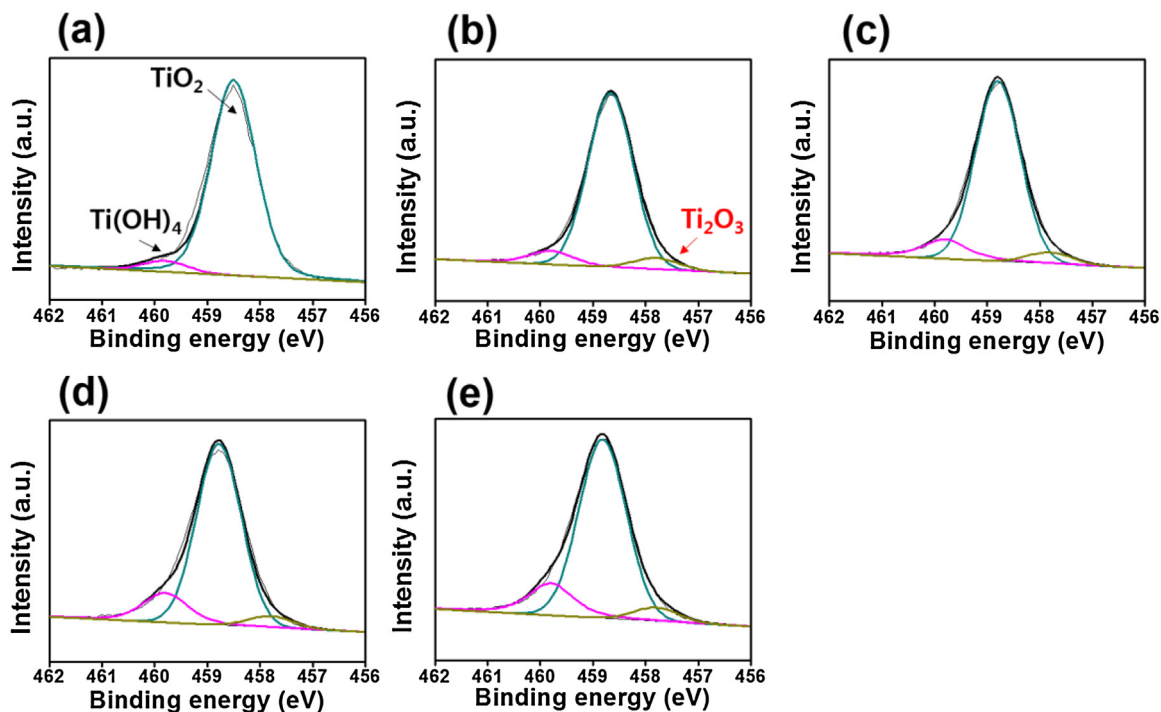

Fig. 5. Ti 2p XPS spectra of (a) a-TiO$_2$, (b) H-TiO$_2$-1.5, (c) H-TiO$_2$-3, (d) H-TiO$_2$-5, and (e) H-TiO$_2$-7.
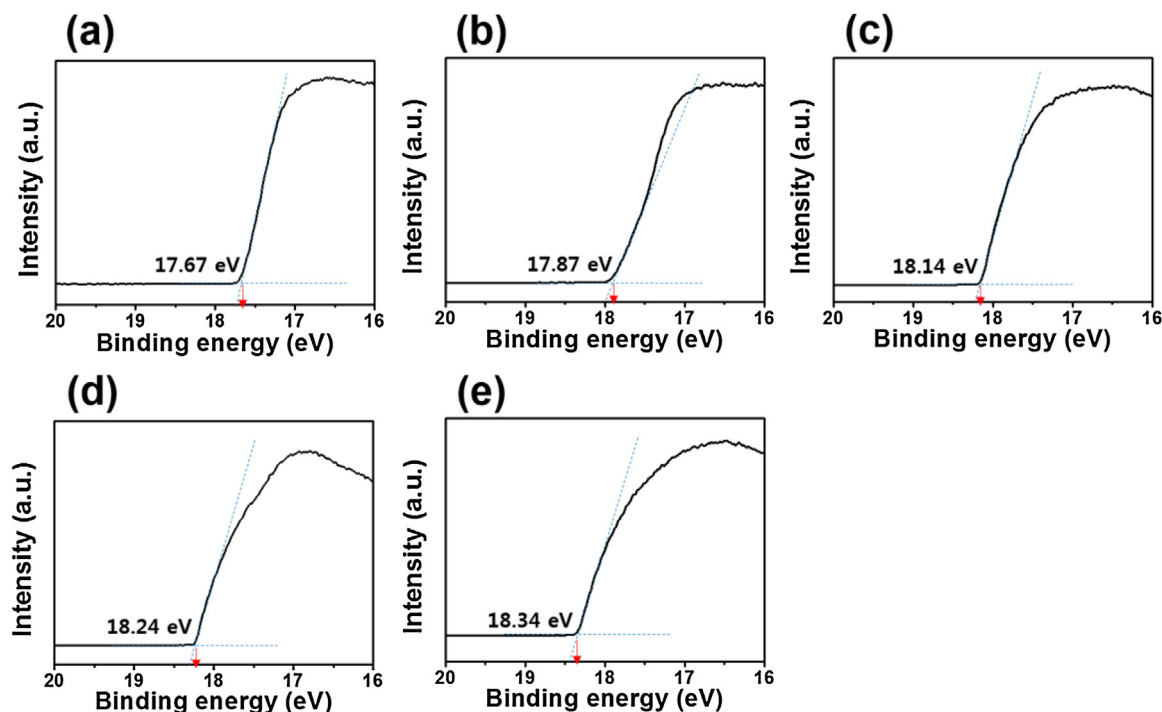
Fig. 6. UPS spectra of (a) a-TiO$_2$, (b) H-TiO$_2$-1.5, (c) H-TiO$_2$-3, (d) H-TiO$_2$-5, and (e) H-TiO$_2$-7 around the secondary electron cutoff region.
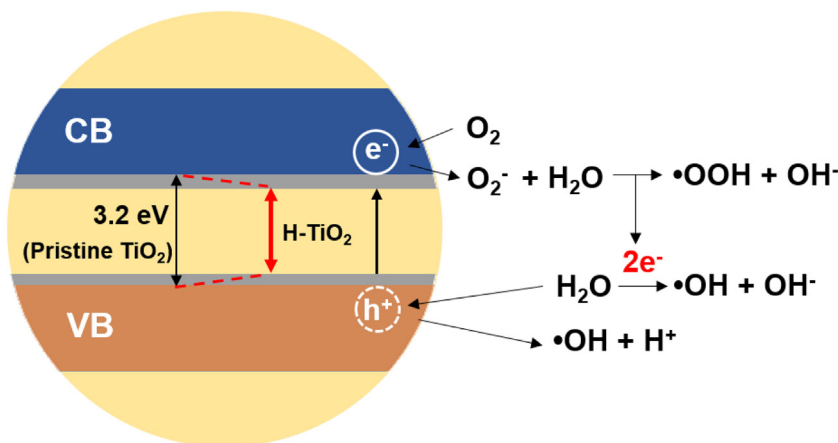

Fig. 7. Schematic of suggested photocatalytic mechanism of H-TiO$_2$ photocatalysts under solar light irradiation.

than a-TiO$_2$. This implies that H$_2$ released from water (H$_2$O) creates different bonding environments of TiO$_2$, such as partial reduction of TiO$_2$ under a reducing atmosphere [33,43]. Fig. 6a–e show the secondary electron cutoffs in UV photoelectron spectroscopy (UPS) spectrum, which were measured to estimate the work function of H-TiO$_2$ photocatalysts obtained under various underwater plasma treatment times. The work function values were ∼3.55 eV for a-TiO$_2$, ∼3.35 eV for H-TiO$_2$-1.5, ∼3.08 eV for H-TiO$_2$-3, ∼2.98 eV for H-TiO$_2$-5, and ∼2.88 eV for H-TiO$_2$-7. This data shows that hydrogenation resulting from underwater plasma created oxygen vacancies, and the resultant oxygen vacancy states lifted the Fermi level and decreased the work function, which could facilitate electron emission and narrow the bandgap [19,44].

On the basis of this, we purposed to increase solar-light absorption using underwater discharge plasma treatment for narrowing the bandgap or forming localized states therein and suggested photocatalytic mechanism for H-TiO$_2$ under solar-light irradiation

(Fig. 7). In general, the enhanced photocatalytic activities of TiO$_2$ are attributed to surface Ti-H bonds that provide improved optical absorption and an efficient photogenerated electron-hole separation [45,46]. Therefore, the Ti—H and Ti—OH bonds generated on the surface of H-TiO$_2$ during the plasma treatment can enhance the charge separation and the oxygen vacancy states formed within the bandgap, and can act as an intermediate to facilitate the charge excitation under the solar light irradiation [15,47–49]. To compare the optical properties of the a-TiO$_2$ and H-TiO$_2$ photocatalysts, the ultraviolet-visible-near infrared (UV–vis-NIR) absorbance (%) between 200 nm and 800 nm was measured as shown in Fig. S3. All the TiO$_2$ samples showed an apparent adsorption in UV-light region below the 400 nm wavelength [46]. Also, the optical absorption of H-TiO$_2$ photocatalysts extends into the visible range with increased oxygen vacancies or Ti^{3+} species, which indicates that the band gaps of H-TiO$_2$ were narrowed during underwater plasma treatment [50].

In particular, $O_2{}^-\bullet$ and $\bullet OH$ free radicals generated in this photocatalytic process attack and degrade organic substrates in water, leading to improved photodegradation potential [51]. To observe the generation of these free radicals, electron spin resonance (ESR) was employed. Fig. 8 presents the ESR spectra of H-TiO$_2$-3 photocatalysts under LED irradiation. H-TiO$_2$-3 shows 1:2:2:1 patterns, implying the production of $\bullet OH$ free radicals [47]. This result indicates the presence of active oxygen species due to underwater plasma treatment, which can enhance the photocatalytic efficiency.

3.2. Photocatalytic degradation of azo dye

H-TiO$_2$ photocatalysts showed high crystallinity, large BET surface area, and narrowed bandgap, which play important roles in improving the photocatalytic performances. A degradation test of RB 5, Rho B, and Ph dye solutions was carried out to demonstrate the photocatalytic performance of the a-TiO$_2$ and H-TiO$_2$ photocatalysts under UV and solar light irradiation. In the basic photocatalytic process, TiO$_2$ absorbs the light with energy larger than its bandgap and generates excited electrons and holes in the conduction band and the valence band, respectively. These excited charges may be separated from each other and migrate to the surface to participate in photocatalytic reactions [33,51]. As shown in Fig. 9a, after 120 min UV irradiation, H-TiO$_2$ photocatalysts exhibited greater degradation efficiency than P25 and a-TiO$_2$, almost completely removing RB 5 (>99% efficiency). The degradation rates,
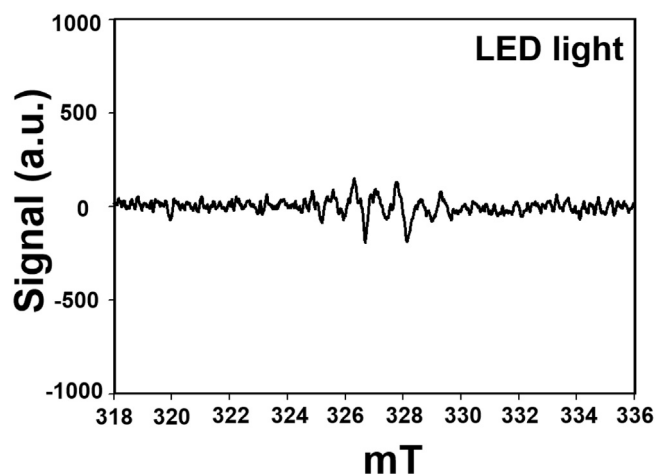

Fig. 8. ESR spectra of H-TiO$_2$-3 photocatalysts under LED irradiation.

k related to the degradation efficiency, were $0.99\,h^{-1}$ for commercial TiO$_2$ (P25), $0.75\,h^{-1}$ for a-TiO$_2$, and $4.60\,h^{-1}$ for H-TiO$_2$ samples. Extra degradation tests of Rho B and Ph under UV irradiation also gave similar results. Fig. 9b–c show that Rho B and Ph were almost completely degraded by H-TiO$_2$ photocatalysts after 120 min UV irradiation. With 120 min solar light irradiation, H-
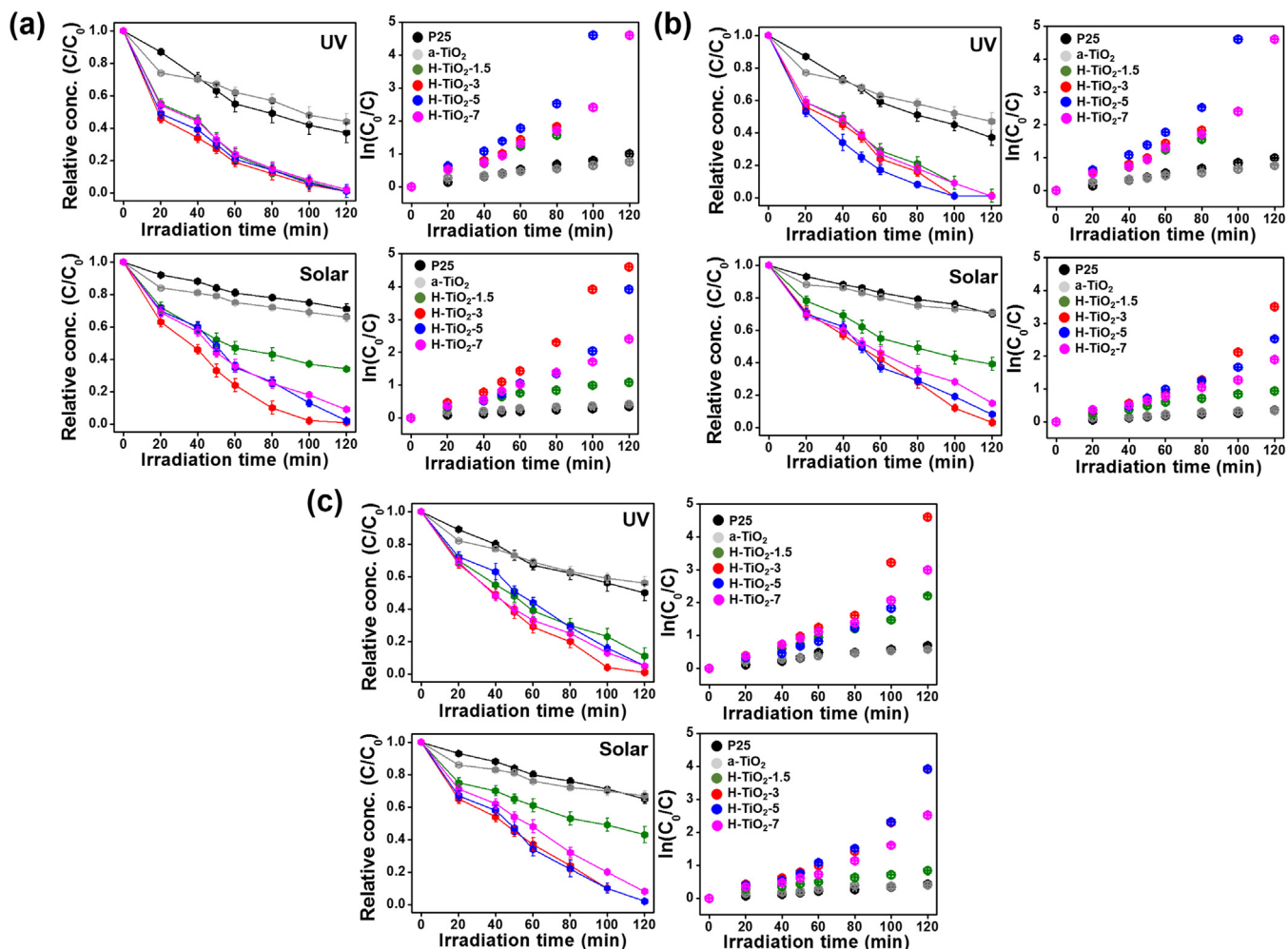

Fig. 9. Removal of (a) reactive black 5 (RB 5), (b) rhodamine B (Rho B), and (c) Phenol (Ph) by commercial TiO$_2$ (P25), a-TiO$_2$, H-TiO$_2$-1.5, H-TiO$_2$-3, H-TiO$_2$-5 and H-TiO$_2$-7 under UV and solar light irradiation.
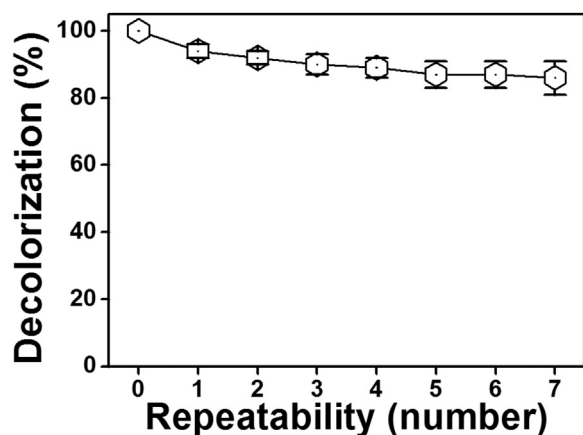
Fig. 10. Recycling results for H-TiO$_2$-3's decolorization of Rho B solution.

TiO$_2$ samples treated with underwater plasma for more than 3 min achieved high degradation of the RB 5, Rho B, and Ph solutions (Fig. 9a–c), while the other photocatalysts (commercial TiO$_2$ and a-TiO$_2$) showed relatively low removal efficiencies. Especially, it seems that the activity of H-TiO$_2$-1.5 under solar light irradiation relatively decreased compared with other H-TiO$_2$ samples. This could be attributable to a large amount of remaining carbon in the sample and/or high work function, which made it difficult to absorb a lot of solar light. Additionally, the removal test of high concentration of Ph (50 mg/L) was conducted under solar light. During 240 min of solar light irradiation, the H-TiO$_2$ samples treated with underwater plasma for more than 3 min showed higher degradation efficiencies of high concentrated phenol solutions than those of the other photocatalysts (Fig. S4). This superb photocatalytic performance of H-TiO$_2$ samples results from their narrowed bandgaps, which lead to the formation of increased numbers of •OH free radicals, and large surface areas offering more available active sites for absorption of azo dye [15,36,46].

Under solar light irradiation, the initial duration was 120 min and decolorization of H-TiO$_2$-3 was measured at the end of each cycle (Fig. 10). After 7 repeatable measurements, the photocatalytic conversion ratio of H-TiO$_2$-3 for Rho B declined to approximately 83% of its original value. It is suggested that the slight decrease of the conversion ratio after each cycle can be due to the loss of H-TiO$_2$-3. Nevertheless, it is certain that H-TiO$_2$ samples are excellent photocatalysts because degradation efficiency is maintained after the repeated cycles.

3.3. Antibacterial activities of H-TiO$_2$ photocatalysts

The antibacterial activities of commercial TiO$_2$ (P25), a-TiO$_2$, and H-TiO$_2$ samples were evaluated for the disinfection of E. coli under solar light irradiation, based on the reduction in the colony numbers of E. coli and S. aureus bacteria formed on LB plates (Fig. 11). Bacterial viability was calculated as viability (%) = $B/A \times 100$ (where the numbers of surviving microbial colonies under the non-illuminated and solar light irradiated conditions were A and B, respectively). After 180 min solar light irradiation, H-TiO$_2$ samples that received underwater plasma treatment for more than 3 min reduced E. coli viabilities to the range 12–18%, whereas somewhat lower bacterial inhibition of E. coli was observed for commercial TiO$_2$ (63%), a-TiO$_2$ (70%), and H-TiO$_2$-1.5 (57%). Likewise, H-TiO$_2$ samples treated by underwater plasma for more than 3 min showed high antibacterial efficiencies (10–19% viabilities) for S. aureus. These results show that H-TiO$_2$ samples treated by underwater plasma for more than 3 min inhibited the growth of E. coli and S. aureus efficiently and their antibacterial performance was enhanced as solar light irradiation times increased. This is because of the high concentration of •OH free radicals on the surface of H-TiO$_2$ samples under solar light irradiation. Previous reports suggest that •OH could be a very strong oxidant species with antimicrobial activity [35]. Thus, these promising antibacterial activities of H-TiO$_2$ may be applied to various useful applications for alternative sterilization technology.

3.4. Highly photocatalytic and antibacterial performances of H-TiO$_2$ photocatalysts

Our results have identified the following factors responsible for the superior photocatalytic and antibacterial efficiencies of H-TiO$_2$ photocatalysts: (1) High crystallinity, which improves their effective utilization by enhancing photocatalytic activity; (2) Large BET surface area, which allows adsorption of more dye molecules on the surface of the photocatalyst, and greater adherence of photocatalyst to bacterial surfaces; (3) Narrow bandgap, which can be achieved that many oxygen species generated by the underwater plasma will form oxygen vacancy states within the bandgap and decrease the work function. This results in bandgap narrowing of the H-TiO$_2$, enabling the absorption of more solar light. Fig. 12 represents the properties of H-TiO$_2$ photocatalysts treated by underwater plasma for 0–7 min in terms of BET and work function, which are important factors determining photocatalytic performance. After the underwater plasma treatment, the BET surface areas were enhanced and the work functions were reduced compared to a-TiO$_2$. Especially, the H-TiO$_2$ photocatalysts treated
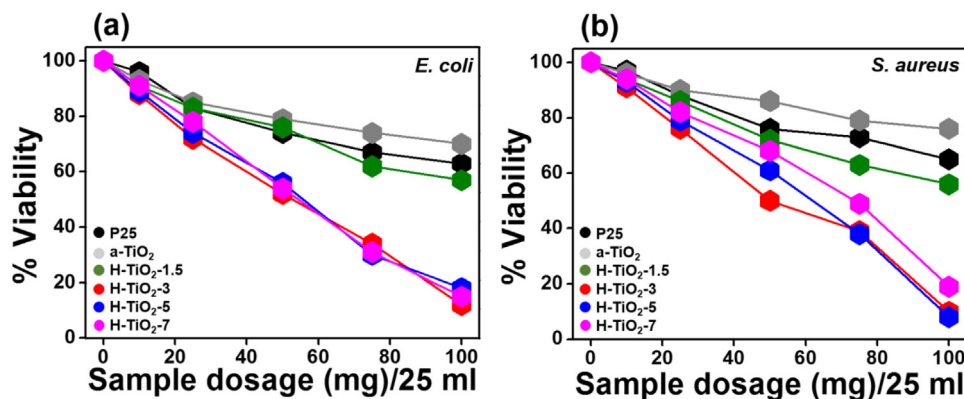

Fig. 11. Plots of cell viability (%) versus solar light irradiation time (min) for commercial TiO$_2$ (P25), a-TiO$_2$, H-TiO$_2$-1.5, H-TiO$_2$-3, H-TiO$_2$-5 and H-TiO$_2$-7 against (a) E. coli and (b) S. aureus.
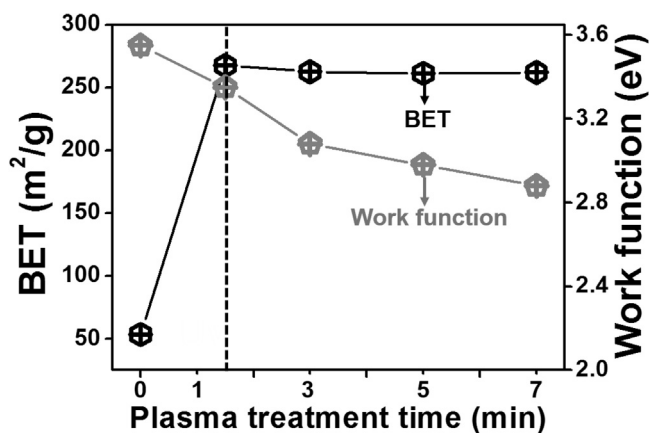
Fig. 12. BET and work function of H-TiO$_2$ photocatalysts prepared with underwater discharge plasma treatment times ranging from 0 to 7 min.

for more than 3 min exhibited almost constant BET values and work functions. This indicates that H-TiO$_2$ with high photocatalytic and antibacterial efficiencies can be obtained by underwater plasma treatment for a short time of only 1–7 min. Therefore, underwater plasma treatment could be considered as a simple and fast hydrogenation method for mass production of superior photocatalytic materials at room temperature.

4. Conclusions

Mass producible nanoporous hydrogenated TiO$_2$ photocatalysts (H-TiO$_2$) were prepared using an underwater plasma treatment system without any thermal processing. Underwater plasma discharge was employed to produce hydrogenated TiO$_2$ photocatalysts with high crystallinity and porous structure suitable for solar irradiation, and able to generate many reactive oxygen species with photocatalytic effects. From the morphological and structural analysis, it was shown that the H-TiO$_2$ photocatalysts were composed of a high bicrystalline phase (anatase/brookite) and displayed large surface area. In particular, XPS and UPS investigations demonstrated that the hydrogenation induced by the underwater plasma generated oxygen vacancies and hydroxyl species resulted in a decreased work function, thereby enhancing electron emission and narrowing the bandgap for photocatalytic activities. Correspondingly, H-TiO$_2$ photocatalysts treated by underwater plasma for more than 3 min showed highly efficient degradation performances for reactive black 5, rhodamine B, and phenol, and excellent efficiencies for disinfection of *E. coli* and *S. aureus* under solar light irradiation. We believe that the development of underwater plasma systems based on hydrogenated TiO$_2$ photocatalysts holds excellent promise for environmental and antibacterial applications.

Acknowledgements

Appendix A. Supplementary data

Supplementary data associated with this article can be found, in the online version, at http://dx.doi.org/10.1016/j.apcatb.2017.04.027.

References

[1] C.-T. Dinh, T.-D. Nguyen, F. Kleitz, T.-O. Do, Shape-controlled synthesis of highly crystalline titania nanocrystals, ACS Nano 3 (2009) 3737–3743.

[2] J. Lu, Y. Dai, H. Jin, B. Huang, Effective increasing of optical absorption and energy conversion efficiency of anatase TiO$_2$ nanocrystals by hydrogenation, Phys. Chem. Chem. Phys. 13 (2011) 18063–18068.

[3] D. Wang, D. Choi, J. Li, Z. Yang, Z. Nie, R. Kou, D. Hu, C. Wang, L.V. Saraf, J. Zhang, I.A. Aksay, J. Liu, Self-assembled TiO$_2$–graphene hybrid nanostructures for enhanced Li-ion insertion, ACS Nano 3 (2009) 907–914.

[4] S. Kurian, H. Seo, H. Jeon, Significant enhancement in visible light absorption of TiO$_2$ nanotube arrays by surface band gap tuning, J. Phys. Chem. C 117 (2013) 16811–16819.

[5] S. Zhang, S. Zhang, B. Peng, H. Wang, H. Yu, H. Wang, F. Peng, High performance hydrogenated TiO$_2$ nanorod arrays as a photoelectrochemical sensor for organic compounds under visible light, Electrochem. Commun. 40 (2014) 24–27.

[6] M. Pelaez, N.T. Nolan, S.C. Pillai, M.K. Seery, P. Falaras, A.G. Kontos, P.S.M. Dunlop, J.W.J. Hamilton, J.A. Byrne, K. O'Shea, M.H. Entezari, D.D. Dionysiou, A review on the visible light active titanium dioxide photocatalysts for environmental applications, Appl. Catal. B Environ. 125 (2012) 331–349.

[7] S. Banerjee, D.D. Dionysiou, S.C. Pillai, Self-cleaning applications of TiO$_2$ by photo-induced hydrophilicity and photocatalysis, Appl. Catal. B Environ. 176–177 (2015) 369–428.

[8] V. Etacheri, C.D. Valentin, J. Schneider, D. Bahnemann, Visible-light activation of TiO$_2$ photocatalysts: advances in theory and experiments, J. Photochem. Photobiol. C: Photochem. Rev. 25 (2015) 1–29.

[9] X. Yu, B. Kim, Y.K. Kim, Highly enhanced photoactivity of anatase TiO$_2$ nanocrystals by controlled hydrogenation-Induced surface defects, ACS Catal. 3 (2013) 2479–2486.

[10] G.-S. Li, E.-Q. Zhang, J.C. Yu, A new visible-light photocatalyst: Cds quantum dots embedded mesoporous TiO$_2$, Environ. Sci. Technol. 43 (2009) 7079–7085.

[11] D. Jiang, Y. Xu, D. Wu, Y. Sun, Visible-light responsive dye-modified TiO$_2$ photocatalyst, J. Solid State Chem. 181 (2008) 593–602.

[12] S.W. Shin, J.Y. Lee, K.-S. Ahn, S.H. Kang, J.H. Kim, Visible light absorbing TiO$_2$ nanotube arrays by sulfur treatment for photoelectrochemical water splitting, J. Phys. Chem. C 119 (2015) 13375–13383.

[13] S. George, S. Pokhrel, Z. Ji, B.L. Henderson, T. Xia, L. Li, J.I. Zink, A.E. Nel, L. Mädler, J. Am. Chem. Soc. 133 (2011) 11270–11278.

[14] Y.-X. Han, C.-L. Yang, M.-S. Wang, X.-G. Ma, L.-Z. Wang, Enhancing the visible-light absorption of TiO$_2$ with the use of key N, Co, and Na dopant concentrations, Sol. Energy Mater. Sol. Cells 132 (2015) 94–100.

[15] H.U. Lee, S.C. Lee, S.H. Choi, B. Son, S.J. Lee, H.J. Kim, J. Lee, Highly visible-light active nanoporous TiO$_2$ photocatalysts for efficient solar photocatalytic applications, Appl. Catal. B: Environ. 129 (2013) 106–113.

[16] F.M. Pesci, G. Wang, D.R. Klug, Y. Li, A.J. Cowan, Efficient suppression of electron–hole recombination in oxygen-deficient hydrogen-treated TiO$_2$ nanowires for photoelectrochemical water splitting, J. Phys. Chem. C 117 (2013) 25837–25844.

[17] X. Chen, L. Liu, Z. Liu, M.A. Marcus, W.-C. Wang, N.A. Oyler, M.E. Grass, B. Mao, P.-A. Glans, P.Y. Yu, J. Guo, S.S. Mao, Properties of disorder-engineered black titanium dioxide nanoparticles through hydrogenation, Sci. Rep. 3 (2013) 1510.

[18] R.E. Rex, F.J. Knorr, J.L. McHale, Comment on characterization of oxygen vacancy associates within hydrogenated TiO$_2$: a positron annihilation study, J. Phys. Chem. C 117 (2013) 7949–7951.

[19] X. Chen, L. Liu, F. Huang, Black titanium dioxide (TiO$_2$) nanomaterials, Chem. Soc. Rev. 44 (2015) 1861–1885.

[20] G. Panomsuwan, A. Watthanaphanit, T. Ishizaki, N. Saito, Water-plasma-assisted synthesis of black titania spheres with efficient visible-light photocatalytic activity, Phys Chem. Chem. Phys. 17 (2015) 13794–13799.

[21] N. Liu, C. Schneider, D. Freitag, M. Hartmann, U. Venkatesan, J. Müller, E. Spiecker, P. Schmuki, Black TiO$_2$ nanotubes: cocatalyst-Free open-circuit hydrogen generation, Nano Lett. 14 (2014) 3309–3313.

[22] C. Xu, Y. Song, L. Lu, C. Cheng, D. Liu, X. Fang, X. Chen, X. Zhu, D. Li, Electrochemically hydrogenated TiO$_2$ nanotubes with improved photoelectrochemical water splitting performance, Nanoscale Res. Lett. 8 (2013) 391.

[23] Z. Wang, C. Yang, T. Lin, H. Yin, P. Chen, D. Wan, F. Xu, F. Huang, J. Lin, X. Xie, M. Jiang, Visible-light photocatalytic, solar thermal and photoelectrochemical properties of aluminium-reduced black titania, Energy Environ. Sci. 6 (2013) 3007–3014.

[24] Y.C. Hong, H.J. Park, B.J. Lee, W.S. Kang, H.S. Uhm, Plasma formation using a capillary discharge in water and its application to the sterilization of *E. coli*, Phys. Plasmas 17 (2010) 053502.

[25] Y.C. Hong, H.W. Jeon, B.J. Lee, H.S. Uhm, Generation of plasma using capillary discharge in water, IEEE Trans. Plasma Sci. 38 (2010) 3464–3466.

[26] Y.J. Kim, Y.C. Hong, S.J. Lee, J.H. Kim, B.J. Lee, H.S. Uhm, Underwater capillary discharge on the penetrability of a membrane, Surf. Coat. Technol. 228 (2013) S482–S485.

[27] J.-L. Brisset, E. Hnatiuc, Peroxynitrite a Re-examination of the chemical properties of non-thermal discharge burning in air over aqueous solutions, plasma chem, Plasma Process. 32 (2012) 655–674.

[28] P. Lukes, E. Dolezalova, I. Sistova, M. Clupek, Auqeous-phase chemistry and bactericidal effects from an air discharge plasma in contact with water:

evidence for the formation of peroxynitrite through a pseudo-second-order post-discharge reaction of H_2O_2 and HNO_2, Plasma Sources Sci. Technol. 23 (2014) 015019.

[29] Y. Nakano, S. Fujimura, T. Sato, T. Kikuchi, M. Ichinose, A. Watanabe, Sterilization method using plasma discharge against biofilm-producing *Pseudomonas aeruginosa* on surface of contact lens, J. Med. Biol. Eng. 35 (2015) 626–633.

[30] K. Shimizu, S. Muramatsu, T. Sonoda, M. Blajan, Water treatment by low voltage discharge in water, J. Plasma Environ. Sci. Technol. 4 (2010) 58–64.

[31] D.B. Graves, The emerging role of reactive oxygen and nitrogen species in redox biology and some implications for plasma applications to medicine and biology, J. Phys. D: App. Phys. 45 (2012) 263001.

[32] J.Y. Huh, K. Kim, C.H. Cho, Y.J. Kim, Y.C. Hong, Characterization of copper nanoparticles synthesized from a plasma discharge in solution, Mater. Focus 3 (2014) 410–414.

[33] H.-R. An, S.Y. Park, H. Kim, C.Y. Lee, S. Choi, S.C. Lee, S. Seo, E.C. Park, Y.-K. Oh, C.-H. Song, J. Won, Y.J. Kim, J. Lee, H.U. Lee, Y.-C. Lee, Advanced nanoporous TiO_2 photocatalysts by hydrogen plasma for efficient solar-light photocatalytic application, Sci. Rep. 6 (2016) 29683.

[34] Z. Qing, Q. Jieshu, P. Hao, T. Luo, Z. Xingfu, Synergistic manipulation of micro-nanostructures and composition: anatase/rutile mixed-phase TiO_2 hollow micro-nanospheres with hierarchical mesopores for photovoltaic and photocatalytic applications, Nanotechnology 22 (2011) 39573.

[35] J. Ding, Z. Huang, J. Zhu, S. Kou, X. Zhang, H. Yang, Low-temperature synthesis of high-ordered anatase TiO_2 nanotube array films coated with exposed {001} nanofacets, Sci. Rep. 5 (2015) 17773.

[36] H.U. Lee, Y.-C. Lee, S.C. Lee, S.Y. Park, B. Son, J.W. Lee, C.-H. Lim, C.-J. Choi, M.-H. Choi, S.Y. Lee, Y.-K. Oh, J. Lee, Visible-light-responsive bicrystalline (anatase/brookite) nanoporous nitrogen-doped TiO_2 photocatalysts by plasma treatment, Chem. Eng. J. 254 (2014) 268–275.

[37] D.H. Hanaor, C.C. Sorrell, Review of the anatase to rutile phase transformation, J. Mater. Sci. 46 (2011) 855–874.

[38] J. Yu, Y. Su, B. Cheng, Template-free fabrication and enhanced photocatalytic activity of hierarchical macro-/mesoporous titania, Adv. Funct. Mater. 17 (2007) 1984–1990.

[39] X.H. Yang, Z. Li, G. Liu, J. Xing, C. Sun, H.G. Yang, C. Li, Ultra-thin anatase TiO_2 nanosheets dominated with {001} facets: thickness-controlled synthesis, growth mechanism and water-splitting properties, Cryst. Eng. Commun. 13 (2011) 1378–1383.

[40] W.F. Zhang, Y.L. He, M.S. Zhang, Z. Yin, Q. Chen, Raman scattering study on anatase TiO_2 nanocrystals, J. Phys. D: Appl. Phys. 33 (2000) 912.

[41] J. Liu, H. Bai, Y. Wang, Z. Liu, X. Zhang, D.D. Sun, Self-assembling TiO_2 nanorods on large graphene oxide sheets at a two-phase interface and their anti-recombination in photocatalytic applications, Adv. Funct. Mater. 20 (2010) 4175–4181.

[42] C.-L. Liang, G.-A. Cheng, R.-T. Zheng, H.-P. Liu, J.-C. Li, H.-F. Zhang, G.-J. Ma, Y.-L. Jiang, Composition and texture of TiN thin films fabricated by ECR enhanced sputtering deposition, Surf. Coat. Technol. 201 (2007) 5537–5540.

[43] Z. Zheng, B. Huang, J. Lu, Z. Wang, X. Qin, X. Zhang, Y. Dai, M.-H. Whangbo, Hydrogenated titania: synergy of surface modification and morphology improvement for enhanced photocatalytic activity, Chem. Commun. 48 (2012) 5733–5735.

[44] W.-D. Zhu, C.-W. Wang, J.-B. Chen, D.-S. Li, F. Zhou, H.-L. Zhang, Enhanced field emission from hydrogenated TiO_2 nanotube arrays, Nanotechnology 23 (2012) 455204.

[45] M.M. Khan, S.A. Ansari, D. Pradhan, M.O. Ansari, D.H. Han, J. Lee, M.H. Cho, Band gap engineered TiO_2 nanoparticles for visible light induced photoelectrochemical and photocatalytic studies, J. Mater. Chem. A 2 (2014) 637–644.

[46] Y. Yan, M. Han, A. Konkin, T. Koppe, D. Wang, T. Andreu, G. Chen, U. Vetter, J.R. Morante, P. Schaaf, Slightly hydrogenated TiO_2 with enhanced photocatalytic performance, J. Mater. Chem. A 2 (2014) 12708–12716.

[47] H.U. Lee, S.C. Lee, J. Won, B.-C. Son, S. Choi, Y. Kim, S.Y. Park, H.-S. Kim, Y.-C. Lee, J. Lee, Stable semiconductor black phosphorus (BP)@titanium dioxide (TiO_2) hybrid photocatalysts, Sci. Rep. 5 (2015) 8691.

[48] H.-U. Lee, K. Ahn, S.-Y. Jeong, C.-R. Cho, J.-P. Kim, J.-S. Bae, H.-G. Kim, S.-H. Kwon, H.W. Lee, Enhanced photocatalytic activity of TiO_2 nanobarbed fibers treated with atmospheric pressure plasma using O_2 gas, Appl. Phys. Lett. 97 (2010) 223111.

[49] X. Xiang, X.-Y. Shi, X.-L. Gao, F. Ji, Y.-J. Wang, C.-M. Liu, X.-T. Zu, Effect of N-doping on absorption and luminescence of anatase TiO_2 films, Chin. Phys. Lett. 29 (2012) 027801.

[50] X. Xin, T. Xu, L. Wang, C. Wang, Ti^{3+}-self doped brookite TiO_2 single-crystalline nanosheets with high solar absorption and excellent photocatalytic CO_2 reduction, Sci. Rep. 6 (2016) 23684.

[51] D. Chatterjee, S. Dasgupta, Visible light induced photocatalytic degradation of organic pollutants, J. Photochem. Photobiol. C: Photochem. Rev. 6 (2005) 186–205.